Laser-induced alignment of weakly bound molecular aggregates

Linda V. Thesing,[1,2,3] Andrey Yachmenev,[1,2] Rosario González-Férez,[4,*] and Jochen Küpper[1,2,3,†]

[1]*Center for Free-Electron Laser Science, Deutsches Elektronen-Synchrotron DESY, Notkestrasse 85, 22607 Hamburg, Germany*

[2]*The Hamburg Center for Ultrafast Imaging, Universität Hamburg, Luruper Chaussee 149, 22761 Hamburg, Germany*

[3]*Department of Physics, Universität Hamburg, Luruper Chaussee 149, 22761 Hamburg, Germany*

[4]*Instituto Carlos I de Física Teórica y Computacional and Departamento de Física Atómica, Molecular y Nuclear, Universidad de Granada, 18071 Granada, Spain*

(Received 3 August 2018; published 12 November 2018)

The rotational and torsional dynamics of the prototypical floppy indole(H_2O) molecular cluster was theoretically and computationally analyzed. The time-dependent Schrödinger equation was solved for a reduced-dimensionality description of the cluster, taking into account overall rotations and the internal rotation of the water moiety. Based on our results, it became clear that the coupling between the internal and the overall rotations is small, and that for typical field strengths in alignment and mixed-field-orientation experiments the rigid-rotor approximation can be employed to describe the investigated dynamics. Furthermore, the parameter space over which this is valid and its boundaries where the coupling of the internal and overall rotation can no longer be neglected were explored.

DOI: 10.1103/PhysRevA.98.053412

I. INTRODUCTION

Biological function is strongly shaped by the intricate interaction of the molecules with their aqueous environment. Unraveling the underlying (bio)molecule-water solvation interactions as well as their relevance for chemical dynamics promises a detailed understanding of their contributions to function. Approaching this through studies of the elementary chemical processes as intrinsic properties in well-defined molecular aggregates enables the definition of fundamental building blocks as a dynamical basis of intermolecular solute-solvent interactions and their chemical dynamics. This rationalizes the longstanding history of detailed studies of molecule-solvent clusters in the gas phase [1,2].

Novel imaging techniques with highest spatiotemporal resolution, such as ultrafast x-ray [3,4] or electron diffraction [5,6], photoelectron imaging [7–9], and laser-induced electron diffraction [10], will provide a new level of detail to these investigations and promise to allow for the recording of molecular movies of the dynamical interactions. The applicability of these imaging methods to complex molecular systems relies on the preparation of pure samples [11,12] and benefits tremendously from fixing the molecules in space [11,13–15], i.e., to align or orient them [16–19]. Recently, some of us have demonstrated the preparation of pure beams of the prototypical indole-water dimer cluster as well as its laser alignment [20–22].

However, it is not clear in how far the very floppy structure of weakly bound molecular clusters modifies or hinders the control techniques, especially regarding alignment with strong laser fields. It is well understood that internal rotation, or torsions, and overall rotation are coupled [23] and that internal rotations can also be controlled with the same strong laser fields [24]. So far, experimental and theoretical studies have been limited to highly symmetric molecular systems [24–28], e.g., with G_{16} symmetry, such as biphenyls. It is *a priori* not clear how these effects will transfer to complex "real world" (bio)molecules and their complexes.

Here, we set out to analyze the laser alignment and the corresponding influence of internal rotations to the overall rotational dynamics of molecule-solvent systems, which, generally, have lower symmetries and asymmetric shapes of the constituents. Specifically, we start these investigations with a theoretical analysis of the laser alignment of the prototypical indole-water dimer systems [29–32], which we treat as a semirigid rotor with an additional one-dimensional internal rotation coordinate corresponding to the rotation of the water moiety about its *b* axis; see Fig. 1. We utilize a reduced-mode variational approach based on the general-molecule variational approach [33–35] combined with a general treatment of electric fields [36].

II. THEORY AND COMPUTATIONAL SETUP

The model structure of indole(H_2O) that is employed in this work is schematically shown in Fig. 1. The water molecule is attached to the planar indole frame via a hydrogen bond where the oxygen atom of the water molecule lies in the indole plane. We treat the indole(H_2O) cluster as a floppy molecule with the water molecule undergoing an internal rotation. The angle of internal rotation τ is defined as the dihedral angle between the indole and the water planes (see Fig. 1), with $\tau = 90^\circ$ in the equilibrium configuration [29]. We keep all other vibrational coordinates fixed at their equilibrium values along the minimum-energy path (MEP) of the internal

*rogonzal@ugr.es

†jochen.kuepper@cfel.de; https://www.controlled-molecule-imaging.org

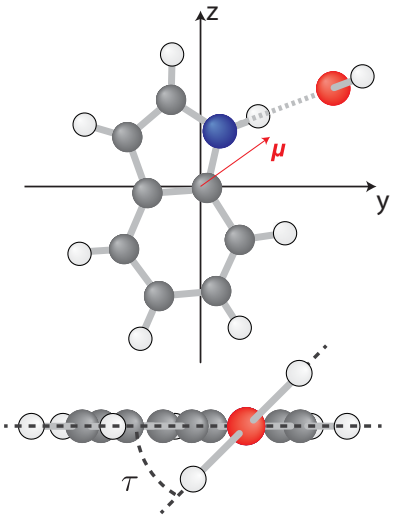

FIG. 1. Sketch of the indole(H_2O) dimer cluster. The most polarizable axis defines the z axis of the molecular frame. The torsional angle is defined as the dihedral angle between the indole and water planes. For the experimentally determined structure, see Ref. [29].

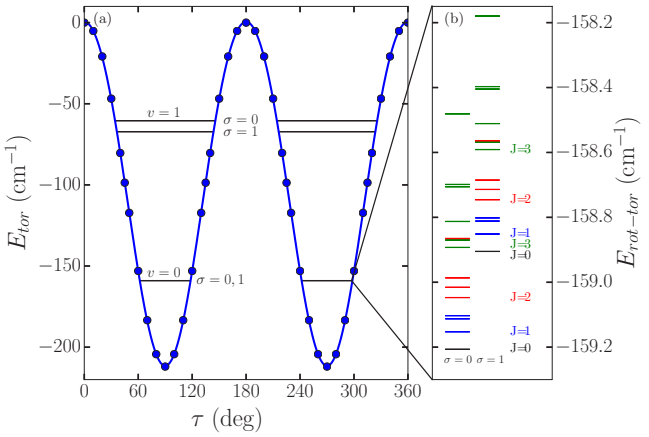

FIG. 2. (a) The *ab initio* 1D potential-energy surface (blue circles) and corresponding fit (blue line) and the lowest two field-free torsional energy levels of indole(H_2O), obtained from the pure torsional part of the Hamiltonian (1). Each torsional level, denoted by the vibrational quantum number v, is split into two sublevels $\sigma = 0, 1$ of opposite parity. (b) Field-free rotation-torsional energy levels for $J = 0, \ldots, 3$ corresponding to the torsional ground state, obtained from the Hamiltonian (1). Due to the small coupling between the internal and overall rotation, the energy levels are approximately given by the sum of the pure torsional and pure rotational energies. Thus, for each J, there are $2J + 1$ rotational energy levels in a given torsional sublevel; see text for more details.

rotation. The MEP is determined by optimizing the structural parameters of the indole(H_2O) complex at different values of the τ coordinate between 0° and 360°.

We assume the Born-Oppenheimer approximation and consider four degrees of freedom, three Euler angles (ϕ, θ, χ) describing the overall rotation of the system, and the angle τ associated with the internal rotation of the water molecule. The field-free Hamiltonian of the system is

$$H_0 = +\frac{1}{2}\sum_{\alpha,\beta=x,y,z} \hat{J}_\alpha G^{\rm rot}_{\alpha\beta}(\tau)\hat{J}_\beta + \frac{1}{2}p_\tau G^{\rm tor}_\tau(\tau)p_\tau + \frac{1}{2}\sum_{\alpha=x,y,z}\left[p_\tau G^{\rm cor}_{\tau\alpha}(\tau)\hat{J}_\alpha + \hat{J}_\alpha G^{\rm cor}_{\alpha\tau}(\tau)p_\tau\right] + V(\tau), \quad (1)$$

where $\hat{J}_\alpha$ are components of the rotational angular momentum operator in the molecule-fixed frame (MFF) and $p_\tau = -i\hbar\partial/\partial\tau$. The kinetic-energy matrices $G^{\rm tor}_\tau(\tau)$ and $G^{\rm rot}_{\alpha\beta}(\tau)$ are associated with the internal torsional and overall rotational motions, $G^{\rm cor}_{\tau\alpha}(\tau)$ describes coupling between the two motions, and $V(\tau)$ is the potential-energy function. The elements of the kinetic-energy matrices are calculated as functions of the torsional coordinate τ following the generalized procedure from TROVE [35,37]. The kinetic-energy matrices and potential-energy function in (1) were built along the MEP. The geometry optimizations were carried out using the density-fitted second-order Møller-Plesset perturbation theory DF-MP2 in the frozen-core approximation, in conjunction with the augmented correlation-consistent basis set aug-cc-pVTZ [38,39]. For the density-fitting approximation, we utilized the JKFIT [40] and MP2FIT [41] auxiliary basis sets specifically matched to aug-cc-pVTZ. All electronic-structure calculations were carried out using PSI4 [42]. The *ab initio* potential-energy surface (PES) is represented by an analytical function by fitting the expression

$$V(\tau) = \sum_{n=0}^{2} V_{2n}\cos(2n\tau). \quad (2)$$

The PES is depicted in Fig. 2(a) and the coefficients are $V_0 = -101.950\ {\rm cm}^{-1}$, $V_2 = 106.006\ {\rm cm}^{-1}$, and $V_4 = -3.58143\ {\rm cm}^{-1}$, in good agreement with the experimental value for this motion of $V_2 = 99\ {\rm cm}^{-1}$ [29]. The structural parameters are represented by similar analytical functions; see Appendix B.

Our analysis is restricted to a nonresonant linearly polarized laser ac electric field combined with a parallel weak dc electric field. The interaction of the polarizability with the weak dc field is neglected. In addition, we can average over the rapid oscillations of the nonresonant ac field and the interaction of the electric-dipole moment with the laser field vanishes. The interaction of the molecule with the external electric fields then reads

$$H_{\rm int}(t) = -\boldsymbol{\mu}(\tau)\cdot\mathbf{E}_{\rm stat} - \tfrac{1}{4}\mathbf{E}_{\rm laser}(t)\underline{\underline{\alpha}}(\tau)\mathbf{E}_{\rm laser}(t), \quad (3)$$

where $\mathbf{E}_{\rm stat}$ is the static electric field and $\mathbf{E}_{\rm laser}(t)$ is the envelope of the laser electric field. The electric-dipole moment (EDM) $\boldsymbol{\mu}(\tau)$ and the polarizability tensor $\underline{\underline{\alpha}}(\tau)$ of indole(H_2O) are calculated along the minimum-energy path created by varying the τ coordinate; see Appendix A. They are represented by analytical functions similar to the ones used for the PES; see Appendix C. The polarization axis of the laser is chosen as the Z axis of the laboratory fixed frame (LFF). The molecule-fixed frame (x, y, z) is defined by the principle axes of polarizability at the equilibrium configuration so that the diagonal elements fulfill $\alpha_{xx} < \alpha_{yy} < \alpha_{zz}$.

To study the rotational dynamics of indole(H_2O), we solve the time-dependent Schrödinger equation (TDSE) for the full Hamiltonian

$$H(t) = H_0 + H_{\rm int}(t), \tag{4}$$

using the short iterative Lanczos method [43,44] for the time propagation and a basis-set expansion for the spatial coordinates using the eigenstates of the field-free Hamiltonian (1). The field-free eigenbasis is calculated variationally in several steps. First, the pure rotational and torsional basis functions, $\Psi_l^{\rm rot}(\phi,\theta,\chi)$ and $\Psi_l^{\rm tor}(\tau)$, are constructed by diagonalizing the respective parts of the field-free Hamiltonian (1). In this step, we use Wang states [45], i.e., symmetrized combinations of symmetric-top functions, as a basis set for the rotational coordinates. For the torsional coordinates, we use sine and cosine functions $\phi_n^{\rm even}(\tau) = \cos(n\tau)/\sqrt{\pi}$ and $\phi_n^{\rm odd}(\tau) = \sin(n\tau)/\sqrt{\pi}$, $n > 0$, and $\phi_0^{\rm even}(\tau) = 1/\sqrt{2\pi}$ to preserve the even and odd symmetry of the states. The matrix elements of the full Hamiltonian (4) are then set up in the product basis $\Psi_l^{\rm rot}(\phi,\theta,\chi)\Psi_m^{\rm tor}(\tau)$ and transformed to the eigenbasis of the complete field-free Hamiltonian (1) following the generalized approach developed in RICHMOL [36].

To analyze the importance of the internal motion of the water molecule, we compare our results to calculations using the rigid-rotor approximation [46], i.e., considering only the three degrees of freedom of the overall rotation in (1). For the rigid-rotor calculations, we use the structural parameters, EDM, and polarizability tensor at the equilibrium configuration, i.e., $\tau = 90^\circ$.

III. RESULTS AND DISCUSSION

In this section, we analyze the overall rotational and torsional dynamics of indole(H_2O). We solve the TDSE using the field-free ground state as the initial state of the time propagation, i.e., $T = 0$ K. For the laser pulse, we consider a Gaussian envelope $\mathbf{E}_{\rm laser}(t) = \hat{\mathbf{e}}_Z E_0 \exp(-4\ln 2 t^2/\tau_{\rm FWHM}^2)$ with $E_0 = 2.74 \times 10^7$ V/cm and $\tau_{\rm FWHM} = 1$ ns. The parallel static electric field is increased to a field strength of $\mathbf{E}_{\rm stat} = 600$ V/cm slowly enough to ensure adiabatic behavior before the laser field is applied. We analyze the alignment and mixed-field-orientation dynamics of indole(H_2O), quantified by the expectation values $\langle\cos^2\theta\rangle$ and $\langle\cos\theta\rangle$, respectively, as well as the torsional alignment $\langle\cos^2\tau\rangle$.

Figures 3(a) and 3(b) show the time evolution of the alignment and orientation of the ground state of indole(H_2O) obtained using the nonrigid rotation-torsional Hamiltonian [thick blue (dark gray) lines] as well as the results using the rigid-rotor approximation [thin red (light gray) lines]. As the laser-field strength rises, the most polarizable axis (MPA) becomes strongly aligned along the polarization axis of the laser, reaching $\langle\cos^2\theta\rangle = 0.98$ at the peak intensity. For both the rigid and nonrigid models, we observe a typical mixed-field-orientation dynamics that has previously been described for other linear and asymmetric top molecules [47–50]. Due to the presence of the static electric field, the orientation increases as laser-aligned pendular states are formed and increasingly coupled with increasing laser-field strength. The orientation at the peak intensity, $\langle\cos\theta\rangle = 0.82$, is lower than the value obtained in the adiabatic description, $\langle\cos\theta\rangle = 0.99$,

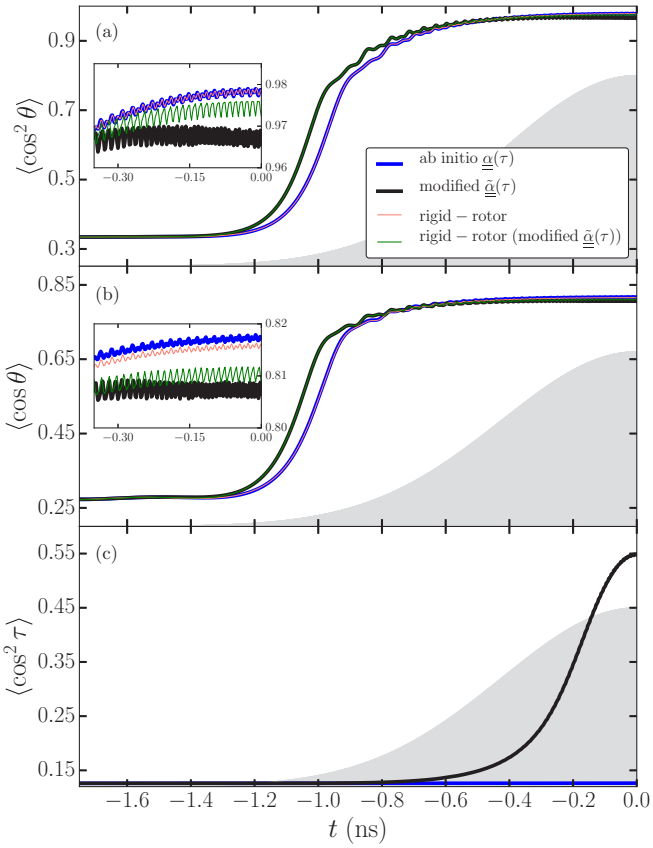

FIG. 3. For the ground state of indole(H_2O) ($T = 0$ K), the time evolution of the expectation values (a) $\langle\cos^2\theta\rangle$, (b) $\langle\cos\theta\rangle$, and (c) $\langle\cos^2\tau\rangle$ using $\underline{\underline{\alpha}}(\tau)$ from *ab initio* calculations [thick blue (dark gray) lines] and the modified $\tilde{\underline{\underline{\alpha}}}(\tau)$ (thick black lines). For comparison, results using the rigid-rotor approximation for the two polarizabilities are shown [thin red (light gray) lines and thin green (gray) lines, respectively]. The results for the *ab initio* polarizability $\underline{\underline{\alpha}}(\tau)$ and the rigid-rotor approximation in (a) and (b) are practically indistinguishable. The smallest values of $\langle\cos^2\theta\rangle$ and $\langle\cos\theta\rangle$ and the largest value of $\langle\cos^2\tau\rangle$ at the peak intensity are obtained for the modified polarizability $\tilde{\underline{\underline{\alpha}}}(\tau)$. The result for the modified polarizability differs from the corresponding rigid-rotor result at the peak intensity. The insets in (a) and (b) show a zoom of $\langle\cos^2\theta\rangle$ and $\langle\cos\theta\rangle$ close to the peak intensity. The gray area illustrates the envelope of the laser field with $E_0 = 2.74 \times 10^7$ V/cm. The static field strength is $\mathbf{E}_{\rm stat} = 600$ V/cm.

indicating a nonadiabatic dynamics, i.e., several field-dressed eigenstates of the instantaneous Hamiltonian (4) contribute to the time-dependent wave function [46,51,52].

We point out that the results obtained for the rigid and nonrigid descriptions are practically identical, which shows that the indole(H_2O) cluster can be treated as a rigid molecule for moderate electric-field strengths that are typically employed in molecular alignment and mixed-field-orientation experiments. To understand why the internal rotation of the water molecule does not influence the overall rotational dynamics, we look at the coupling between the internal and overall rotations and the resulting rotation-torsional energy levels. In the field-free case, the coupling of the two motions is described by the off-diagonal blocks $G_{\tau\alpha}^{\rm cor}(\tau)$ of the kinetic-

TABLE I. Coefficients of the analytical functions (C1) used to fit the modified polarizability. The components α_{12} and α_{23} are zero.

n	$\tilde{\alpha}_n^{(11)}$ (a.u.)	$\tilde{\alpha}_n^{(13)}$ (a.u.)	$\tilde{\alpha}_n^{(22)}$ (a.u.)	$\tilde{\alpha}_n^{(33)}$ (a.u.)
0	98.8163	56.5324	−9.156292	193.5136
1	−23.5024	49.02866	−77.91074	47.57616

energy matrix and the dependence of $G_{\alpha\beta}^{\mathrm{rot}}(\tau)$ on the torsional angle τ in (1). Since this field-free coupling is very small [29], the eigenstates of the Hamiltonian (1) are approximately described by the product states $\Psi_l^{\mathrm{rot}}(\phi,\theta,\chi)\Psi_m^{\mathrm{tor}}(\tau)$, and the energy levels are given approximately by the sum of the pure rotational and torsional energies (Fig. 2), even for large values of the quantum number J. Due to tunneling, each torsional level splits into two sublevels, denoted by $\sigma = 0, 1$ in Fig. 2(a). The energy difference between two consecutive torsional states is three orders of magnitude larger than the energy gaps between pure rotational states. As a result, the rotation-torsional energy levels are distributed as bands of rotational states for each torsional sublevel; see Fig. 2(b).

In the presence of external electric fields, the internal and overall rotations are additionally coupled due to the dependence of the EDM and the polarizability on the torsional angle [see (3)], which is weak for indole(H_2O). Thus, for the ac and dc field strengths considered here, the field-induced coupling between the torsional ground and first-excited state $\langle\Psi_{i,v=0}^{\mathrm{rot-tor}}|H_{\mathrm{int}}|\Psi_{j,v=1}^{\mathrm{rot-tor}}\rangle$, where $v = 0, 1$ indicates the torsional ground and excited state, respectively, is small ($<1\ \mathrm{cm}^{-1}$) compared to the energy gap $\Delta E \approx 98\ \mathrm{cm}^{-1}$ between these torsional levels. Due to the symmetry of the EDM and the polarizability, the two sublevels $\sigma = 0, 1$ of a torsional state are not coupled by the external electric fields; see Appendix D. As a consequence, the field-dressed rotation-torsional wave packet is dominated by the torsional ground state. The torsional alignment shown in Fig. 3(c) [thick blue (dark gray) lines] thus remains constant with $\langle\cos^2\tau\rangle = 0.126$. To achieve a field-induced coupling that is strong enough to overcome the energy gap between the torsional ground and first-excited state, laser-field strengths larger than $E_0 \approx 10^8$ V/cm, i.e., intensities $I_{\mathrm{control}} > 10^{13}\ \mathrm{W/cm}^2$, would be necessary. Such fields would, however, affect the electronic structure and induce ionization of indole(H_2O) and are generally not used to control the rotational dynamics of these clusters [21].

In the following, we investigate for which regimes of field-free and field-induced couplings the rigid-rotor approximation can still be applied to describe the rotational dynamics. To obtain a large field-induced coupling, stronger external ac and dc electric fields could be applied or the dependence of the EDM and the polarizability on the torsional angle τ could be, artificially, increased. We begin by studying a molecular cluster that has a modified polarizability $\underline{\tilde{\alpha}}(\tau)$ and is otherwise identical to indole(H_2O). Since the interaction with the weak static electric field is much weaker than the one with the laser field, we do not modify the EDM. We set $\tilde{\alpha}_{pq}(\tau)$ including only terms with $n \leqslant 1$ (see Appendix C) and with the coefficients listed in Table I. The coefficients $\tilde{\alpha}_2^{(pq)}$ are chosen to be 200 times larger than the largest ones obtained from fits to the *ab initio* results. The chosen $\tilde{\alpha}_0^{(pq)}$ satisfy $\underline{\tilde{\alpha}}(\tau = 90^\circ) = \underline{\alpha}(\tau = 90^\circ)$. This polarizability increases the field-induced coupling by a similar magnitude as increasing the laser-field strength by a factor of $\sqrt{200}$. We carry out an additional rigid-rotor calculation using the structural parameters and EDM at the equilibrium configuration, but the expectation values $\langle\tilde{\alpha}_{pq}\rangle = \langle\Psi_0^{\mathrm{tor}}|\tilde{\alpha}_{pq}(\tau)|\Psi_0^{\mathrm{tor}}\rangle$ in the torsional ground state as these values differ significantly from $\tilde{\alpha}_{pq}(\tau = 90^\circ)$. We point out that the expectation value of the modified polarizability is not diagonal in the chosen MFF, i.e., the MPA of the modified polarizability is not parallel to the MFF z axis.

The results for this enhanced-response molecular system are depicted in Fig. 3 for the nonrigid-rotor (black lines) and rigid-rotor [thin green (gray) lines] cases. At lower laser-field strengths, the alignment does not differ from the results obtained using the rigid-rotor approximation. Close to the peak intensity, the alignment starts to decrease and reaches a value of $\langle\cos^2\theta\rangle = 0.965$, slightly smaller than the rigid rotor result $\langle\cos^2\theta\rangle = 0.972$. Simultaneously, the orientation starts to differ slightly from the rigid-rotor result reaching a smaller value at the peak intensity. Regarding the torsional alignment, we observe an increase of $\langle\cos^2\tau\rangle$ with increasing laser-field strength due to the contribution of excited torsional states, in particular the second-excited state $v = 2, \sigma = 0$. The reason for this is that due to the symmetry of the polarizability, the coupling between the field-free rotation-torsional states with different torsional symmetry is small [20,53]; see Appendix D. The difference between the nonrigid- and the rigid-rotor descriptions can be understood in terms of the effective polarizability $\langle\Psi_m^{\mathrm{tor}}|\underline{\tilde{\alpha}}(\tau)|\Psi_m^{\mathrm{tor}}\rangle$ of the torsional states. For weak laser fields, excited torsional states are not involved in the dynamics. As a consequence, the alignment and orientation evolve in a similar way as for the rigid indole(H_2O). The torsional ground-state wave function is localized around $\tau = 90^\circ$, yielding a polarizability with small off-diagonal elements $\langle\tilde{\alpha}_{13}\rangle = \langle\tilde{\alpha}_{31}\rangle = 5.2$ a.u.; $\tilde{\alpha}_{13}(\tau = 90^\circ) = 0$. At stronger laser fields, the contributions of excited torsional states modify the polarizability, with $\langle\tilde{\alpha}_{13}\rangle = 23.5$ a.u. at the peak intensity. As a result, a different molecular axis is aligned compared to the rigid-rotor case and $\langle\cos^2\theta\rangle$ decreases. In addition to the change in the MPA, the anisotropy of the polarizability increases with increasing laser-field strength. The alignment of the MPA $\langle\cos^2\theta_{\mathrm{MPA}}\rangle$, where θ_{MPA} is the angle between the MPA and the LFF Z axis, is thus larger at the peak intensity than for the rigid-rotor case. As a result of the change in the MPA, the orientation $\langle\cos\theta\rangle$ in Fig. 3(b) also decreases, but a larger orientation of the MPA $\langle\cos\theta_{\mathrm{MPA}}\rangle$ is obtained for the nonrigid than for the rigid case.

Additionally modifying the EDM in an analogous way results in different effective dipole moments $\langle\boldsymbol{\mu}\rangle$ and a correspondingly changed degree of orientation compared to the rigid-rotor result. However, since the interaction of the dc electric field with the dipole moment is comparably weak, no additional excitation of torsional states occurs. Increasing the laser-field strength by the corresponding factor of $\sqrt{200}$ does not have the same impact on the rotational dynamics as the modified polarizability. While a stronger laser field leads to contributions of excited torsional states, the expectation value of the polarizability in these excited states does not differ much from the one in the torsional ground state. Thus, no

significant change of the MPA or polarizability anisotropy occurs. Calculations performed for a laser-field strength of $E_0 = 3 \times 10^8$ V/cm and $\mathbf{E}_{\text{stat}} = 0$ show a small increase in $\langle \cos^2 \tau \rangle$ during the laser pulse, but no difference in the overall alignment $\langle \cos^2 \theta \rangle$ between the rigid and nonrigid descriptions. Increasing the laser-field strength further was computationally too expensive.

In addition to analyzing the impact of a strong field-induced coupling, we investigate the influence of the barrier height. This affects the torsional energy-level structure [23] and may thus alter the field-dressed coupling necessary to achieve an excitation of the torsion in the presence of external fields. To this end, we use a modified torsional potential $\tilde{V}(\tau) = \tilde{V}_0[\cos(2\tau) - 1]$ with a very small barrier height $\tilde{V}_0 = 1.0\ \text{cm}^{-1}$. Using the same field parameters as in Fig. 3 and the *ab initio* polarizability, we observe an overall rotational dynamics that is very similar to the dynamics obtained using the *ab initio* torsional potential. The reason for this is that by lowering the barrier height, the energy gap between the torsional ground and second-excited level is only decreased to $\Delta E \approx 55\ \text{cm}^{-1}$, which is still large compared to the coupling induced by the external electric fields. Finally, we consider molecules with an internal rotor that has a smaller rotational constant. For a modified molecular system increasing the mass of the protons in the water molecule of indole(H_2O) to 14 u and keeping the *ab initio* polarizability, the rotational dynamics for the rigid and nonrigid descriptions are almost indistinguishable when applying the field configuration as in Fig. 3. If we additionally consider a low torsional barrier with $\tilde{V}_0 = 1.0\ \text{cm}^{-1}$ (see above), the energy gap between the torsional ground state and second-excited state is lowered to $\Delta E \approx 4.5\ \text{cm}^{-1}$ and we observe contributions of excited torsional states. Here, the field-free rotation-torsional states belonging to the excited torsional levels cannot be approximated well as product states of pure rotational and torsional states. As a consequence, the orientation slightly differs from the rigid-rotor result with $\Delta \langle \cos \theta \rangle = 0.01$.

IV. SUMMARY AND CONCLUSIONS

We investigate the rotational dynamics of a floppy molecule in combined laser and static electric fields. Our work is focused on the prototypical indole(H_2O) cluster where the attached water molecule undergoes an internal rotation. The molecular structure, electric-dipole moment, and polarizability are calculated with *ab initio* methods. We solve the time-dependent Schrödinger equation for a moderate laser-field strength and a weak dc electric field taking into account four degrees of freedom for the internal and overall rotation. We compare the obtained alignment and orientation dynamics to results computed within the rigid-rotor approximation. We demonstrate that indole(H_2O) can be treated as a rigid molecule in typical alignment and mixed-field-orientation experiments. This conclusion is rationalized by the weak field-free and field-induced couplings of the internal and overall motions compared to the respective energy spacings. We explore regimes of laser-field strengths for which the internal rotation of the water moiety can no longer be neglected. However, such strong laser pulses, $I_{\text{control}} > 10^{13}\ \text{W/cm}^2$, are not likely to be used in alignment experiments as they would result in electronic excitation and ionization. Let us remark that even at a rotational temperature of $T = 0$ K, both torsional sublevels $\sigma = 0, 1$ of the rotational ground state would be populated in a molecular beam according to their nuclear spin statistical weights. However, as the rotational and torsional dynamics of these two sublevels in the presence of the ac and dc fields do not differ significantly, our analysis of the $\sigma = 0$ sublevel provides a good description of the overall rotational dynamics in the external fields.

We analyze the influence of a larger field-induced coupling on the overall and internal rotational dynamics by using artificially modified electric-dipole moment and polarizability with a two-orders-of-magnitude-stronger dependence on the torsional angle. We find a decrease of the overall alignment and orientation close to the peak intensity due to an effective change in the MPA in the excited torsional state. In addition, we observe an increase of the torsional alignment with increasing laser-field strength caused by the contributions of excited torsional states. In contrast, for unmodified indole(H_2O), a constant torsional alignment is found.

Based on these results for indole(H_2O), we conclude that similar molecular clusters can also be treated as rigid molecules. This conclusion can also be extended to other floppy molecular systems provided their dipole moment and polarizability depend only weakly on the internal motion and their rotational and torsional energy levels are approximately given by the sum of pure rotational and torsional energies with large gaps between consecutive torsional levels. For molecules with a small torsional barrier or a smaller internal rotational constant, e.g., for previously studied biphenyl-type molecules, a weaker field-induced coupling may already lead to contributions of excited torsional states to the field-dressed dynamics. However, the rigid-rotor approximation can still be employed for moderate laser-field strengths. This is different than for previously studied biphenyl-type molecules, which have their axis of internal rotation parallel to a principle axis of inertia and their MPA not modified by the torsion, which results in a qualitatively different coupled rotational and torsional dynamics than for generic low-symmetry molecular clusters, such as indole(H_2O). To achieve an accurate description of the rotational dynamics for molecules with small energy gaps between the torsional ground and excited states, the coupling of the internal and overall rotations cannot be neglected. Furthermore, for impulsive alignment, even the small coupling between the internal and overall rotation in indole(H_2O) becomes important on longer, e.g., nanosecond, timescales since the revivals of the alignment are sensitive even to small energy shifts of the field-free rotational states in the wave packet.

The variational approach applied in this work allows one to extend our study to include multiple internal modes in a multidimensional PES and to study their effect on the field-dressed rotational dynamics, which will be investigated in the future.

ACKNOWLEDGMENTS

This work has been supported by the Deutsche Forschungsgemeinschaft (DFG) through the excellence cluster "The Hamburg Center for Ultrafast Imaging – Structure, Dynamics

and Control of Matter at the Atomic Scale" (CUI, Grant No. EXC1074) and through the priority program "Quantum Dynamics in Tailored Intense Fields" (Grants No. QUTIF, No. SPP1840, No. KU 1527/3), by the European Research Council under the European Union's Seventh Framework Programme (Grant No. FP7/2007-2013) through the Consolidator Grant COMOTION (Grant No. ERC-614507-Küpper), and by the Helmholtz Association "Initiative and Networking Fund". R.G.F. gratefully acknowledges financial support by the Spanish Project No. FIS2014-54497-P (MINECO) and by the Andalusian research group FQM-207.

APPENDIX A: *AB INITIO* RESULTS

The *ab initio* results for the components of the EDM $\boldsymbol{\mu}(\tau)$ and polarizability $\underline{\underline{\alpha}}(\tau)$ are depicted in Fig. 4 together with the analytical functions fitted to the *ab initio* results; see Appendix C. For each geometry obtained for a fixed value of the torsional angle, the EDM and polarizability are calculated as first and second derivatives of the electronic energy with respect to external electric fields along the corresponding axis. We use electric-field strengths of $+0.005$ a.u. and -0.005 a.u., where 1 a.u. $= 5.14 \times 10^9$ V/cm. As for the geometry optimization, the DF-MP2 method and aug-cc-pVTZ basis set is used.

APPENDIX B: ANALYTICAL EXPRESSIONS FOR THE STRUCTURAL PARAMETERS

The bond lengths r_i, angles a_i, and dihedral angles d_i of indole(H_2O) are defined in Z matrix form according to Table II, where $d_{18} = \tau$, $d_i = 0$ for $i \in \{4, 5, 7, 8, 9\}$ and $d_i = \pi$ for $i \in \{6, 10, 11, 12, 13, 14, 15, 16, 17, 19\}$. The coordinates r_i, $i \neq 18, 19$, and a_i, $i \neq 18$, are represented as analytical functions of the torsional angle similar to the potential-energy surface,

$$x_i = \sum_{n=0}^{3} x_{2n}^{(i)} \cos(2n\tau), \tag{B1}$$

to preserve their symmetry. To obtain expressions for $r_{18} = r_{OH_1}$, $r_{19} = r_{OH_2}$, and $a_{18} = a_{NOH_1}$, we fit symmetrized coordinates defined as $r_+ = (r_{18} + r_{19})/2$, $r_- = (r_{18} - r_{19})/2$, and $a_- = a_{18} + a_{19}/2 - \pi$, where $a_{19} = a_{HOH}$. For r_+, the expression (B1) is used and for r_- and a_-, we fit

$$x_i = \sum_{n=0}^{2} x_{2n+1}^{(i)} \cos[(2n+1)\tau]. \tag{B2}$$

Analytical expressions for the coordinates r_{18}, r_{19}, and a_{18} are then obtained from those for the symmetrized coordinates. The coefficients $x_{2n}^{(i)}$ and $x_{2n+1}^{(i)}$ are listed in Table III.

TABLE II. Z matrix for internal coordinates of indole(H_2O) as used in the input of the *ab initio* calculations.

C						
C	1	r_2				
C	2	r_3	1	a_3		
C	3	r_4	2	a_4	1	d_4
N	1	r_5	2	a_5	3	d_5
C	2	r_6	1	a_6	3	d_6
C	6	r_7	2	a_7	1	d_7
C	7	r_8	6	a_8	2	d_8
C	8	r_9	7	a_9	6	d_9
H	3	r_{10}	2	a_{10}	1	d_{10}
H	4	r_{11}	3	a_{11}	2	d_{11}
H	6	r_{12}	2	a_{12}	1	d_{12}
H	7	r_{13}	6	a_{13}	2	d_{13}
H	8	r_{14}	7	a_{14}	6	d_{14}
H	9	r_{15}	8	a_{15}	7	d_{15}
O	5	r_{16}	1	a_{16}	2	d_{16}
H	5	r_{17}	1	a_{17}	2	d_{17}
H	16	r_{18}	5	a_{18}	1	d_{18}
H	16	r_{19}	18	a_{19}	5	d_{19}

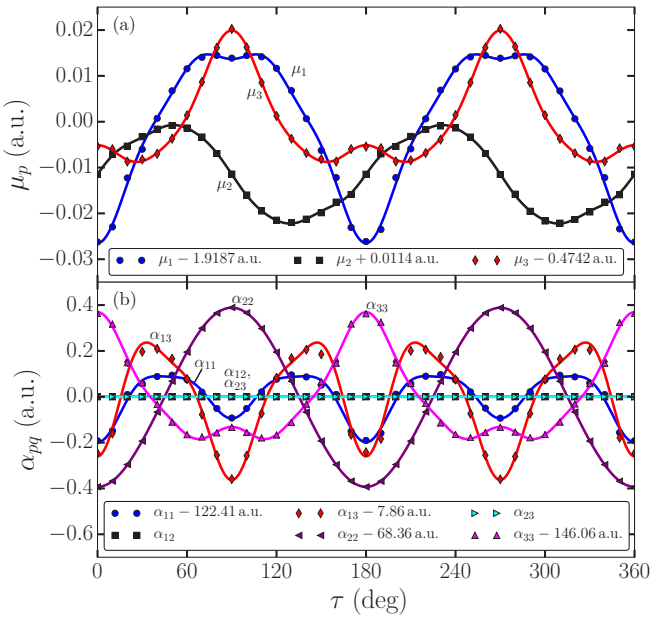

FIG. 4. The *ab initio* results for the components of (a) the EDM $\boldsymbol{\mu}(\tau)$ and (b) the polarizability $\underline{\underline{\alpha}}(\tau)$ (symbols). The solid lines are the analytical functions fitted to the *ab initio* results; see Appendix C.

APPENDIX C: ANALYTICAL EXPRESSIONS FOR THE ELECTRIC-DIPOLE MOMENT AND POLARIZABILITY

To represent $\boldsymbol{\mu}(\tau)$ and $\underline{\underline{\alpha}}(\tau)$ by analytical functions of τ, we transform their components to a coordinate system fixed to the molecular bond structure. The first unit vector $\hat{e}_1$ is chosen along the N-O bond axis, the second one $\hat{e}_2$ is perpendicular to the indole plane, and the third one is given by $\hat{e}_3 = \hat{e}_1 \times \hat{e}_2$. Similar to the fit of the PES, we fit the following expressions to the *ab initio* results of $\boldsymbol{\mu}(\tau)$ and $\underline{\underline{\alpha}}(\tau)$:

$$\mu_p = \sum_{n=0}^{4} \mu_{2n}^{(p)} \cos(2n\tau)\,, \quad \alpha_{pq} = \sum_{n=0}^{4} \alpha_{2n}^{(pq)} \cos(2n\tau), \tag{C1}$$

with $p \in \{1, 3\}$ and $pq \in \{11, 22, 33, 13\}$ as well as

$$\mu_2 = \sin(2\tau) \sum_{n=0}^{4} \mu_{2n}^{(p)} \cos(2n\tau). \tag{C2}$$

The coefficients $\mu_{2n}^{(p)}$ and $\alpha_{2n}^{(pq)}$ are listed in Table IV.

TABLE III. Coefficients of the analytical functions (B1) and (B2) used to fit the internal coordinates computed with *ab initio* methods.

x_i	$x_0^{(i)}$	$x_1^{(i)}$	$x_2^{(i)}$	$x_3^{(i)}$	$x_4^{(i)}$	$x_5^{(i)}$	$x_6^{(i)}$
r_2	1.4165	0.0000	1.1241×10^{-4}	0.0000	-2.4354×10^{-5}	0.0000	7.9153×10^{-7}
r_3	1.4190	0.0000	-1.5673×10^{-4}	0.0000	-6.2654×10^{-6}	0.0000	-2.3140×10^{-6}
r_4	1.3723	0.0000	-5.2534×10^{-6}	0.0000	1.1913×10^{-5}	0.0000	-2.0983×10^{-6}
r_5	1.3653	0.0000	-1.9057×10^{-4}	0.0000	-1.8848×10^{-5}	0.0000	-4.9656×10^{-6}
r_6	1.3996	0.0000	-1.9349×10^{-5}	0.0000	1.2147×10^{-6}	0.0000	-2.3413×10^{-6}
r_7	1.3798	0.0000	-3.3917×10^{-5}	0.0000	3.2087×10^{-6}	0.0000	-7.9436×10^{-7}
r_8	1.4048	0.0000	-5.2823×10^{-5}	0.0000	-1.4796×10^{-6}	0.0000	-4.7037×10^{-6}
r_9	1.3811	0.0000	-4.8092×10^{-5}	0.0000	1.2176×10^{-5}	0.0000	3.4123×10^{-6}
r_{10}	1.0751	0.0000	-1.4861×10^{-5}	0.0000	-1.0067×10^{-6}	0.0000	-4.9208×10^{-7}
r_{11}	1.0752	0.0000	-5.7300×10^{-6}	0.0000	-4.9008×10^{-6}	0.0000	-2.9040×10^{-6}
r_{12}	1.0798	0.0000	-2.7355×10^{-6}	0.0000	3.3204×10^{-6}	0.0000	2.1854×10^{-6}
r_{13}	1.0797	0.0000	-1.7141×10^{-5}	0.0000	8.4508×10^{-6}	0.0000	1.3853×10^{-6}
r_{14}	1.0795	0.0000	6.4960×10^{-7}	0.0000	-2.0485×10^{-5}	0.0000	-1.7834×10^{-6}
r_{15}	1.0800	0.0000	1.9670×10^{-5}	0.0000	8.2218×10^{-6}	0.0000	6.9811×10^{-7}
r_{16}	2.9378	0.0000	1.4169×10^{-2}	0.0000	-1.2038×10^{-4}	0.0000	-4.9276×10^{-5}
r_{17}	1.0090	0.0000	4.6907×10^{-5}	0.0000	4.8672×10^{-7}	0.0000	3.1249×10^{-6}
r_{18}	9.5964×10^{-1}	1.6137×10^{-5}	-3.7570×10^{-5}	-2.3695×10^{-6}	-1.7981×10^{-5}	7.0582×10^{-7}	-2.5055×10^{-6}
r_{19}	9.5964×10^{-1}	-1.6137×10^{-5}	-3.7570×10^{-5}	2.3695×10^{-6}	-1.7981×10^{-5}	-7.0582×10^{-7}	-2.5055×10^{-6}
a_3	1.8649	0.0000	3.7557×10^{-5}	0.0000	-5.1228×10^{-5}	0.0000	-1.1234×10^{-6}
a_4	1.8647	0.0000	-1.7675×10^{-4}	0.0000	4.1198×10^{-5}	0.0000	1.2049×10^{-6}
a_5	1.8773	0.0000	1.8366×10^{-6}	0.0000	6.5937×10^{-5}	0.0000	1.5983×10^{-6}
a_6	2.0751	0.0000	2.8057×10^{-4}	0.0000	-3.9346×10^{-5}	0.0000	1.3686×10^{-5}
a_7	2.0749	0.0000	2.0874×10^{-4}	0.0000	2.1963×10^{-6}	0.0000	2.3899×10^{-6}
a_8	2.1167	0.0000	-1.8787×10^{-4}	0.0000	2.3553×10^{-5}	0.0000	-3.4979×10^{-6}
a_9	2.1152	0.0000	-2.1611×10^{-4}	0.0000	-2.4107×10^{-5}	0.0000	-6.0503×10^{-6}
a_{10}	2.2269	0.0000	-1.1047×10^{-4}	0.0000	4.6785×10^{-5}	0.0000	-1.6861×10^{-5}
a_{11}	2.2678	0.0000	-7.3596×10^{-4}	0.0000	-3.7692×10^{-5}	0.0000	1.2068×10^{-5}
a_{12}	2.1047	0.0000	-1.6749×10^{-4}	0.0000	2.1358×10^{-5}	0.0000	1.1809×10^{-6}
a_{13}	2.0896	0.0000	1.6504×10^{-4}	0.0000	-7.4212×10^{-6}	0.0000	-2.8143×10^{-7}
a_{14}	2.0825	0.0000	1.8096×10^{-4}	0.0000	6.1563×10^{-5}	0.0000	8.5536×10^{-6}
a_{15}	2.1148	0.0000	-1.8007×10^{-3}	0.0000	2.2403×10^{-4}	0.0000	-4.2819×10^{-5}
a_{16}	2.1705	0.0000	-2.6675×10^{-4}	0.0000	-8.9622×10^{-3}	0.0000	-1.2984×10^{-3}
a_{17}	2.1885	0.0000	8.9775×10^{-4}	0.0000	-9.4758×10^{-4}	0.0000	1.1903×10^{-5}
a_{18}	2.2242	-4.7488×10^{-2}	9.8120×10^{-4}	-1.5970×10^{-3}	-4.1175×10^{-5}	-4.0832×10^{-3}	1.0285×10^{-5}
a_{19}	1.8347	0.0000	-1.9624×10^{-3}	0.0000	8.2349×10^{-5}	0.0000	-2.0570×10^{-5}

APPENDIX D: SYMMETRY PROPERTIES AND COUPLING DUE TO EXTERNAL ELECTRIC FIELDS

We summarize the symmetry properties of indole(H_2O) and the coupling of different rotation-torsional states in the presence of parallel nonresonant laser and weak static electric fields. In the field-free case, indole(H_2O) belongs to the molecular symmetry group $G_4 = \{E, (12), E^*, (12)^*\}$ [20,29,53]. The static electric field mixes field-free states of different parity and the molecular symmetry group of indole(H_2O) in the field reduces to $G_2 = \{E, (12)\}$ [20]. In terms of the product states $\Psi_l^{\rm rot}(\phi, \theta, \chi)\Psi_m^{\rm tor}(\tau)$, the matrix elements of the two parts of the interaction Hamiltonian (3) depend on $\langle\Psi_m^{\rm tor}|\mu_i(\tau)|\Psi_n^{\rm tor}\rangle$ and $\langle\Psi_m^{\rm tor}|\alpha_{ij}(\tau)|\Psi_n^{\rm tor}\rangle$ with $i, j \in x, y, z$, respectively. Since the dipole moment and polarizability do not change sign under the operation (12), rotation-torsional states with different σ are not coupled by

TABLE IV. Coefficients of the analytical functions (C1) and (C2) used to fit the EDM and polarizability computed with *ab initio* methods. The components α_{12} and α_{23} are zero.

n	$\mu_{2n}^{(1)}$ (a.u.)	$\mu_{2n}^{(2)}$ (a.u.)	$\mu_{2n}^{(3)}$ (a.u.)	$\alpha_{2n}^{(11)}$ (a.u.)	$\alpha_{2n}^{(13)}$ (a.u.)	$\alpha_{2n}^{(22)}$ (a.u.)	$\alpha_{2n}^{(33)}$ (a.u.)
0	1.91872	1.146652×10^{-2}	4.742808×10^{-1}	122.4133	7.866651	68.36602	146.069
1	1.897090×10^{-2}	1.110871×10^{-3}	1.161703×10^{-2}	3.613539×10^{-2}	8.455194×10^{-2}	3.895537×10^{-1}	2.378808×10^{-1}
2	4.952774×10^{-3}	1.531671×10^{-3}	6.384580×10^{-3}	1.17512×10^{-1}	2.451433×10^{-1}	-1.195350×10^{-3}	9.374843×10^{-2}
3	1.113748×10^{-3}	6.033855×10^{-4}	8.993579×10^{-4}	1.584098×10^{-2}	3.293678×10^{-2}	1.155859×10^{-3}	1.251454×10^{-2}
4	1.443935×10^{-3}	5.059124×10^{-4}	1.0173×10^{-3}	2.897917×10^{-2}	6.613491×10^{-2}	-1.084440×10^{-3}	2.512222×10^{-2}

the external ac and dc electric fields. The nonzero components of the polarizability are of A_1 symmetry in G_4 and thus only couple field-free torsional states that have the same symmetry. Since the field-free rotation-torsional states are linear combinations of states with the same rotation-torsional symmetry and only approximately described by product states, the coupling due to the laser field (which is the dominant interaction) between field-free states with different torsional symmetry is nonzero, but smaller than the coupling between states with the same torsional symmetry. Here, the torsional symmetry of a field-free rotation-torsional state refers to the product state $\Psi_l^{\mathrm{rot}}(\phi,\theta,\chi)\Psi_m^{\mathrm{tor}}(\tau)$ with the largest contribution. For parallel laser and static electric fields, M is a good quantum number and we have to distinguish the cases $M=0$ and $M\neq 0$.

If $M\neq 0$, we find two different symmetry species corresponding to states with A and B symmetry in G_2.

For $M=0$, the interaction of the laser field with the polarizability as well as the interaction of the static electric field with the y and z components of the dipole moment couple field-free rotational states with the same $J+K_c$ parity. The y and z components of the dipole moment are of A_1 symmetry in G_4 and thus only couple field-free torsional states with the same symmetry. The x component of the dipole moment is of A_2 symmetry and couples field-free torsional states with different parity, i.e., A_1 and A_2 torsional states as well as B_1 and B_2 states. For $M=0$, the interaction with the x component of the dipole moment couples field-free rotational states with different $J+K_c$ parity. As a consequence, we find two different symmetry species for each value of σ. The two cases for $\sigma=0$ are listed in Table V.

TABLE V. Symmetry species $+$ and $-$ for $M=0$ and $\sigma=0$ in the presence of parallel ac and dc electric fields. The torsional symmetry Γ_{tor} and K_c quantum number refer to the product state $\Psi_l^{\mathrm{rot}}(\phi,\theta,\chi)\Psi_m^{\mathrm{tor}}(\tau)$ that approximately describes a given field-free rotation-torsional state. To obtain the $M=0$ symmetry species for the $\sigma=1$ sublevels, $A_{1,2}$ has to be replaced with $B_{1,2}$.

J	K_c	Γ_{tor}	$\Gamma_{\mathrm{rot}}\otimes\Gamma_{\mathrm{tor}}$	Symmetry species
e	e	A_1	A_1	$+$
o	e	A_1	A_1	$-$
e	o	A_1	A_2	$-$
o	o	A_1	A_2	$+$
e	e	A_2	A_2	$-$
o	e	A_2	A_2	$+$
e	o	A_2	A_1	$+$
o	o	A_2	A_1	$-$

[1] T. S. Zwier, The spectroscopy of solvation in hydrogen-bonded aromatic clusters, Annu. Rev. Phys. Chem. **47**, 205 (1996).

[2] P. S. Cremer, A. H. Flood, B. C. Gibb, and D. L. Mobley, Collaborative routes to clarifying the murky waters of aqueous supramolecular chemistry, Nat. Chem. **10**, 8 (2018).

[3] J. C. H. Spence and H. N. Chapman, The birth of a new field, Philos. Trans. R. Soc. B **369**, 20130309 (2014).

[4] J. Küpper, S. Stern, L. Holmegaard, F. Filsinger, A. Rouzée, A. Rudenko, P. Johnsson, A. V. Martin, M. Adolph, A. Aquila, S. Bajt, A. Barty, C. Bostedt, J. Bozek, C. Caleman, R. Coffee, N. Coppola, T. Delmas, S. Epp, B. Erk, L. Foucar, T. Gorkhover, L. Gumprecht, A. Hartmann, R. Hartmann, G. Hauser, P. Holl, A. Hömke, N. Kimmel, F. Krasniqi, K.-U. Kühnel, J. Maurer, M. Messerschmidt, R. Moshammer, C. Reich, B. Rudek, R. Santra, I. Schlichting, C. Schmidt, S. Schorb, J. Schulz, H. Soltau, J. C. H. Spence, D. Starodub, L. Strüder, J. Thøgersen, M. J. J. Vrakking, G. Weidenspointner, T. A. White, C. Wunderer, G. Meijer, J. Ullrich, H. Stapelfeldt, D. Rolles, and H. N. Chapman, X-Ray Diffraction from Isolated and Strongly Aligned Gas-Phase Molecules with a Free-Electron Laser, Phys. Rev. Lett. **112**, 083002 (2014).

[5] C. J. Hensley, J. Yang, and M. Centurion, Imaging of Isolated Molecules with Ultrafast Electron Pulses, Phys. Rev. Lett. **109**, 133202 (2012).

[6] J. Yang, M. Guehr, X. Shen, R. Li, T. Vecchione, R. Coffee, J. Corbett, A. Fry, N. Hartmann, C. Hast, K. Hegazy, K. Jobe, I. Makasyuk, J. Robinson, M. S. Robinson, S. Vetter, S. Weathersby, C. Yoneda, X. Wang, and M. Centurion, Diffractive Imaging of Coherent Nuclear Motion in Isolated Molecules, Phys. Rev. Lett. **117**, 153002 (2016).

[7] M. Meckel, D. Comtois, D. Zeidler, A. Staudte, D. Pavičić, H. C. Bandulet, H. Pépin, J. C. Kieffer, R. Dörner, D. M. Villeneuve, and P. B. Corkum, Laser-induced electron tunneling and diffraction, Science **320**, 1478 (2008).

[8] C. Z. Bisgaard, O. J. Clarkin, G. Wu, A. M. D. Lee, O. Geßner, C. C. Hayden, and A. Stolow, Time-resolved molecular frame dynamics of fixed-in-space CS_2 molecules, Science **323**, 1464 (2009).

[9] L. Holmegaard, J. L. Hansen, L. Kalhøj, S. L. Kragh, H. Stapelfeldt, F. Filsinger, J. Küpper, G. Meijer, D. Dimitrovski, M. Abu-samha, C. P. J. Martiny, and L. B. Madsen, Photoelectron angular distributions from strong-field ionization of oriented molecules, Nat. Phys. **6**, 428 (2010).

[10] C. I. Blaga, J. Xu, A. D. DiChiara, E. Sistrunk, K. Zhang, P. Agostini, T. A. Miller, L. F. DiMauro, and C. D. Lin, Imaging ultrafast molecular dynamics with laser-induced electron diffraction, Nature (London) **483**, 194 (2012).

[11] F. Filsinger, G. Meijer, H. Stapelfeldt, H. Chapman, and J. Küpper, State- and conformer-selected beams of aligned and oriented molecules for ultrafast diffraction studies, Phys. Chem. Chem. Phys. **13**, 2076 (2011).

[12] Y.-P. Chang, D. A. Horke, S. Trippel, and J. Küpper, Spatially-controlled complex molecules and their applications, Int. Rev. Phys. Chem. **34**, 557 (2015).

[13] J. C. H. Spence and R. B. Doak, Single Molecule Diffraction, Phys. Rev. Lett. **92**, 198102 (2004).

[14] A. Barty, J. Küpper, and H. N. Chapman, Molecular imaging using x-ray free-electron lasers, Annu. Rev. Phys. Chem. **64**, 415 (2013).

[15] K. L. Reid, Accessing the molecular frame through strong-field alignment of distributions of gas phase molecules, Philos. Trans. R. Soc. A **376**, 20170158 (2018).

[16] H. Stapelfeldt and T. Seideman, Colloquium: Aligning molecules with strong laser pulses, Rev. Mod. Phys. **75**, 543 (2003).

[17] O. Ghafur, A. Rouzée, A. Gijsbertsen, W. K. Siu, S. Stolte, and M. J. J. Vrakking, Impulsive orientation and alignment of quantum-state-selected NO molecules, Nat. Phys. **5**, 289 (2009).

[18] L. Holmegaard, J. H. Nielsen, I. Nevo, H. Stapelfeldt, F. Filsinger, J. Küpper, and G. Meijer, Laser-Induced Alignment and Orientation of Quantum-State-Selected Large Molecules, Phys. Rev. Lett. **102**, 023001 (2009).

[19] F. Filsinger, J. Küpper, G. Meijer, L. Holmegaard, J. H. Nielsen, I. Nevo, J. L. Hansen, and H. Stapelfeldt, Quantum-state selection, alignment, and orientation of large molecules using static electric and laser fields, J. Chem. Phys. **131**, 064309 (2009).

[20] S. Trippel, Y.-P. Chang, S. Stern, T. Mullins, L. Holmegaard, and J. Küpper, Spatial separation of state- and size-selected neutral clusters, Phys. Rev. A **86**, 033202 (2012).

[21] S. Trippel, J. Wiese, T. Mullins, and J. Küpper, Communication: Strong laser alignment of solvent-solute aggregates in the gas-phase, J. Phys. Chem. **148**, 101103 (2018).

[22] S. Trippel, M. Johny, T. Kierspel, J. Onvlee, H. Bieker, H. Ye, T. Mullins, L. Gumprecht, K. Długołęcki, and J. Küpper, Knife edge skimming for improved separation of molecular species by the deflector, Rev. Sci. Instrum. **89**, 096110 (2018).

[23] W. Gordy and R. L. Cook, *Microwave Molecular Spectra*, 3rd ed. (Wiley, New York, 1984).

[24] C. B. Madsen, L. B. Madsen, S. S. Viftrup, M. P. Johansson, T. B. Poulsen, L. Holmegaard, V. Kumarappan, K. A. Jørgensen, and H. Stapelfeldt, Manipulating the Torsion of Molecules by Strong Laser Pulses, Phys. Rev. Lett. **102**, 073007 (2009).

[25] L. H. Coudert, L. F. Pacios, and J. Ortigoso, Rotation-Induced Breakdown of Torsional Quantum Control, Phys. Rev. Lett. **107**, 113004 (2011).

[26] S. Ramakrishna and T. Seideman, Torsional Control by Intense Pulses, Phys. Rev. Lett. **99**, 103001 (2007).

[27] T. Grohmann, M. Leibscher, and T. Seideman, Laser-Controlled Torsions: Four-Dimensional Theory and the Validity of Reduced Dimensionality Models, Phys. Rev. Lett. **118**, 203201 (2017).

[28] L. Christensen, J. H. Nielsen, C. B. Brandt, C. B. Madsen, L. B. Madsen, C. S. Slater, A. Lauer, M. Brouard, M. P. Johansson, B. Shepperson, and H. Stapelfeldt, Dynamic Stark Control of Torsional Motion by a Pair of Laser Pulses, Phys. Rev. Lett. **113**, 073005 (2014).

[29] T. M. Korter, D. W. Pratt, and J. Küpper, Indole-H_2O in the gas phase. Structures, barriers to internal motion, and $S_1 \leftarrow S_0$ transition moment orientation. Solvent reorganization in the electronically excited state, J. Phys. Chem. A **102**, 7211 (1998).

[30] J. R. Carney, F. C. Hagemeister, and T. S. Zwier, Hydrogen-bonding topologies of indole-$(water)_n$ clusters from resonant ion-dip infrared spectroscopy, J. Chem. Phys. **108**, 3379 (1998).

[31] M. Mons, I. Dimicoli, B. Tardivel, F. Piuzzi, V. Brenner, and P. Millié, Site dependence of the binding energy of water to indole: Microscopic approach to the side chain hydration of tryptophan, J. Phys. Chem. A **103**, 9958 (1999).

[32] S. Blanco, J. Lopez, J. Alonso, P. Ottaviani, and W. Caminati, Pure rotational spectrum and model calculations of indole-water, J. Chem. Phys. **119**, 880 (2003).

[33] G. O. Sørensen, A new approach to the Hamiltonian of nonrigid molecules, in *Large Amplitude Motion in Molecules II* (Springer Verlag, Berlin, 1979), p. 97.

[34] E. Mátyus, G. Czakó, and A. G. Császár, Toward black-box-type full- and reduced-dimensional variational (ro)vibrational computations, J. Chem. Phys. **130**, 134112 (2009).

[35] S. N. Yurchenko, W. Thiel, and P. Jensen, Theoretical ROVibrational energies (TROVE): A robust numerical approach to the calculation of rovibrational energies for polyatomic molecules, J. Mol. Spectrosc. **245**, 126 (2007).

[36] A. Owens and A. Yachmenev, RichMol: A general variational approach for rovibrational molecular dynamics in external electric fields, J. Chem. Phys. **148**, 124102 (2018).

[37] A. Yachmenev and S. N. Yurchenko, Automatic differentiation method for numerical construction of the rotational-vibrational Hamiltonian as a power series in the curvilinear internal coordinates using the Eckart frame, J. Chem. Phys. **143**, 014105 (2015).

[38] T. H. Dunning, Gaussian basis sets for use in correlated molecular calculations. I. The atoms boron through neon and hydrogen, J. Chem. Phys. **90**, 1007 (1989).

[39] R. A. Kendall, T. H. Dunning, Jr., and R. J. Harrison, Electron affinities of the first-row atoms revisited. Systematic basis sets and wave functions, J. Chem. Phys. **96**, 6796 (1992).

[40] F. Weigend, A fully direct RI-HF algorithm: Implementation, optimised auxiliary basis sets, demonstration of accuracy and efficiency, Phys. Chem. Chem. Phys. **4**, 4285 (2002).

[41] C. Hättig, Optimization of auxiliary basis sets for RI-MP2 and RI-CC2 calculations: Core-valence and quintuple-ζ basis sets for H to Ar and QZVPP basis sets for Li to Kr, Phys. Chem. Chem. Phys. **7**, 59 (2005).

[42] R. M. Parrish, L. A. Burns, D. G. A. Smith, A. C. Simmonett, A. E. DePrince, E. G. Hohenstein, U. Bozkaya, A. Y. Sokolov, R. Di Remigio, R. M. Richard, J. F. Gonthier, A. M. James, H. R. McAlexander, A. Kumar, M. Saitow, X. Wang, B. P. Pritchard, P. Verma, H. F. Schaefer, K. Patkowski, R. A. King, E. F. Valeev, F. A. Evangelista, J. M. Turney, T. D. Crawford, and C. D. Sherrill, Psi4 1.1: An open-source electronic structure program emphasizing automation, advanced libraries, and interoperability, J. Chem. Theory Comput. **13**, 3185 (2017).

[43] C. Leforestier, R. H. Bisseling, C. Cerjan, M. D. Feit, R. Friesner, A. Guldberg, A. Hammerich, G. Jolicard, W. Karrlein, H.-D. Meyer, N. Lipkin, O. Roncero, and R. Kosloff, A comparison of different propagation schemes for the time dependent Schrödinger equation, J. Comput. Phys. **94**, 59 (1991).

[44] M. Beck, A. Jäckle, G. Worth, and H.-D. Meyer, The multiconfiguration time-dependent-Hartree (MCTDH) method: A highly efficient algorithm for propagating wave packets, Phys. Rep. **324**, 1 (2000).

[45] S. C. Wang, On the asymmetrical top in quantum mechanics, Phys. Rev. **34**, 243 (1929).

[46] J. J. Omiste and R. González-Férez, Theoretical description of mixed-field orientation of asymmetric top molecules: a time-dependent study, Phys. Rev. A **94**, 063408 (2016).

[47] J. H. Nielsen, H. Stapelfeldt, J. Küpper, B. Friedrich, J. J. Omiste, and R. González-Férez, Making the Best of Mixed-Field Orientation of Polar Molecules: A Recipe for Achieving

Adiabatic Dynamics in An Electrostatic Field Combined with Laser Pulses, Phys. Rev. Lett. **108**, 193001 (2012).

[48] S. Trippel, T. Mullins, N. L. M. Müller, J. S. Kienitz, R. González-Férez, and J. Küpper, Two-State Wave Packet for Strong Field-Free Molecular Orientation, Phys. Rev. Lett. **114**, 103003 (2015).

[49] J. J. Omiste and R. González-Férez, Nonadiabatic effects in long-pulse mixed-field orientation of a linear polar molecule, Phys. Rev. A **86**, 043437 (2012).

[50] J. J. Omiste and R. González-Férez, Rotational dynamics of an asymmetric-top molecule in parallel electric and nonresonant laser fields, Phys. Rev. A **88**, 033416 (2013).

[51] J. J. Omiste, M. Gaerttner, P. Schmelcher, R. González-Férez, L. Holmegaard, J. H. Nielsen, H. Stapelfeldt, and J. Küpper, Theoretical description of adiabatic laser alignment and mixed-field orientation: the need for a non-adiabatic model, Phys. Chem. Chem. Phys. **13**, 18815 (2011).

[52] L. V. Thesing, J. Küpper, and R. González-Férez, Time-dependent analysis of the mixed-field orientation of molecules without rotational symmetry, J. Chem. Phys. **146**, 244304 (2017).

[53] G. Berden, W. L. Meerts, M. Schmitt, and K. Kleinermanns, High resolution UV spectroscopy of phenol and the hydrogen bonded phenol-water cluster, J. Chem. Phys. **104**, 972 (1996).